Tectonophysics
November 2012, Volume 578 Pages 50-62
http://dx.doi.org/10.1016/j.tecto.2011.10.010
http://archimer.ifremer.fr/doc/00116/22750/

P-wave velocity structure of the southern Ryukyu margin east of Taiwan: Results from the ACTS wide-angle seismic experiment

Klingelhoefer Frauke [1, *], Berthet T. [2], Lallemand S. [2], Schnurle Philippe [1], Lee C. -S. [3], Liu C. -S. [4], Mcintosh K., Theunissen T. [2]

[1] IFREMER, Dep Marine Geosci, Ctr Brest, F-29280 Plouzane, France.
[2] Univ Montpellier 2, CNRS, Geosci Montpellier, F-34095 Montpellier 5, France.
[3] NTOU, Dept Geophys, Keelung, Taiwan.
[4] NTU, Inst Oceanog, Taipei, Taiwan.

* Corresponding author : Frauke Klingelhoefer, email address : fklingel@ifremer.fr

Abstract :

An active seismic experiment has been conducted across the southern Ryukyu margin east of Taiwan over the whole trench-arc-backarc system in May 2009. Twenty-four ocean bottom seismometers (OBS) were deployed from the Ryukyu trench to the southern Okinawa trough over the Ryukyu arc and forearc. Wide angle seismic data were recorded by the OBS array while coincident reflection seismic data were acquired using a 6 km long streamer and a 6600 cubic inch seismic airgun array. Results from tomographic inversion of 21091 travel time picks along this line allowed us to image crustal structures of the Ryukyu margin down to a depth of 25 km. The transect has been designed to provide a better seismic velocity structure of the subduction zone in a highly deformed area that has produced an M8 earthquake in 1920. The line crosses a seismic cluster of earthquakes which source mechanisms are still poorly understood. The subducting oceanic crust of the Huatung Basin is about 5-6 km thick. The underlying mantle exhibits low seismic velocities around 7.8 km/s suggesting some hydrothermal alterations or alteration of the upper mantle through faults generated by the flexure of the subducting plate as it enters the subduction. Low velocities, up to 4.5 km/s, associated with the accretionary wedge are well imaged from the trench back to the Nanao forearc. A major result concerns the abrupt termination of the buttress at the rear of the accretionary wedge. Despite the low resolution of the tomographic inversion near the subduction interface, several lines of evidence supporting the presence of a low velocity zone beneath the toe of the forearc buttress could be established. The Moho beneath the Ryukyu non-volcanic arc is located at a depth around 25 km depth. (C) 2011 Elsevier B.V. All rights reserved.

Highlights

► This paper presents new deep seismic data from a profile across the southern Ryukyu margin east of Taiwan. ► Results from tomographic inversion allows to image crustal structures of the Ryukyu margin down to a depth of 25 km. ► The subducting oceanic crust is about 5-6 km thick and the underlying mantle exhibits relatively low seismic velocities. ► The buttress of the accretionary wedge ends abruptly and some evidence supports a low velocity zone at the forearc. ► The Moho beneath the Ryukyu non-volcanic arc is located at a depth around 25 km depth.

Keywords : Ryukyu Trench, Marine seismics, Wide-angle seismics, Subduction processes

1. Introduction and previous work

The Philippine Sea plate (PSP) converges toward the Eurasia plate (EP) near Taiwan at a rate close to 8 cm/yr in a WNW direction [*Seno et al.*, 1993; *Yu et al.*, 1997]. East of Taiwan, the PSP subducts northward beneath the southern Ryukyu arc (Figure 1). The north-trending PSP slab edge, carrying the extinct north Luzon volcanic arc, is sharply traced by the interruption of its Benioff zone beneath northern Taiwan along 121 degree 30 minutes E. The PSP abuts in this region against either the east-subducting EP slab in depth or the Taiwan orogen at crustal levels. The southernmost Ryukyu subduction zone is thus highly deforming in response to the arc-continent collision that occurs in Taiwan. As a consequence, the forearc area east of the island records a very high level of seismicity [e.g., *Chen et al.*, 2009], with some clustering along probable active faults [e.g., *Font and Lallemand*, 2009]. The largest instrumentally recorded earthquake occurred in this region in 1920. *Theunissen et al.* [2010] have recently proposed a revised magnitude (Mw 7.7 $\pm$ 0.2), location (30 km east of Hualien) and mechanism (thrust) for this event. *Hsu and Sibuet* [2005] have suggested that the southern Ryukyu subduction zones had similar geometrical and tectonic characteristics than the Andaman subduction zone that underwent a giant Mw 9.2 event in 2004. One of the main aims of this work is thus to better image the crustal structure in this area in order to better constrain the source of the seismicity.

One of the first wide-angle seismic surveys conducted south of Taiwan constrained the nature of the crust in the South China Sea Basin to be oceanic and bounded to the north and south by continental type crust [*Ludwig et al.*, 1979]. From modelling of three wide-

angle seismic lines, *Murauchi et al.* [1968] deduced, that the crust underlying the Okinawa Trough is generally similar to that of continental crust, with a Moho depth of 12 km in the eastern Okinawa Trough thinning towards the northwest. *Leyden et al.* [1973] correlated offshore refraction velocities with onland drilling and refraction data to propose a crustal structure in the Okinawa Trough. Based on models from wide-angle seismic data, *Hagen et al.* [1988] propose the nature of the crust east of Taiwan and south of the Ryukyu Trench to be oceanic and continental north of the trench. *Lee et al.* [1980] using two ship seismic refraction lines, found that the Okinawa trough is underlain by a roughly 9 km thick crust, which is overlain by an acoustic basement layer and a 1-2 km thick layer of sediments.

In 1995 a large scale land-sea wide-angle seismic experiment was carried out east and south of Taiwan using the R/V Maurice Ewing for reflection seismic data acquisition and the R/V Ocean Researcher 1 for deployment and recovery of the instruments [*Yeh et al.*, 1998]. One of these regional profiles, oriented north-south, spans from the Okinawa Trough over the Ryukyu Arc and onto the Philippine Sea Plate (Figure 1) [*Wang et al.*, 2001, 2004]. This profile (line 1), which is located in our study area, but oriented in a different angle, images a sudden increase in subduction angle of the PSP below the Nanao forearc basin. Moho depth at the Ryukyu Arc is around 30 km, and around 13 km at the PSP. Three profiles oriented roughly east-west (Lines 14, 16 and 23) were each extended on land. Preliminary modelling of southern Line 23 covering the Luzon Arc shows thickening of the PSP towards the EP, but no indications of a westward subduction of the PSP [*Hetland and Wu*, 1998; *Yang and Wang*, 1998] as previously proposed by *Chemenda et al.* [1997]. Line 14 crosses our profile in the forearc area and is located roughly parallel

to the Ryukyu Arc. Modelling of the OBS data along this profile indicates a poorly constrained Moho depth near 30 km in the vicinity of our profile leading to a crustal thickness larger than 25 km. Sedimentary layers thicken in the Nanao and East Nanao Basin and the continental basement of the Ryukyu arc has been interpreted to terminates beneath the accretionary wedge at a distance of 60 km from the trench [*McIntosh and Nakamura*, 1998; *Wang et al.*, 2001]. However, *McIntosh et al.* [2005], demonstrated that thickened crust was limited to the extinct North Luzon Arc. East of this, at the base of the slope, the OBS data require normal to slightly thin oceanic crust. They found no evidence of significant deformation east of the arc. Line 16, sub-parallel to Line 14 in the forearc (see Figure 1) images the top of the subducting PSP at depths between 20 and 25 km [*Wang and Chiang*, 1998; *McIntosh et al.*, 2005].

An active seismic cluster has been imaged in the forearc area using relocations of 1139 events recorded on both taiwanese and japanese landstations from 1992 and 1997 in a 3D velocity model [*Font et al.*, 2003; *Font and Lallemand*, 2009]. These clustered events mainly align with geomorphological features such as the Hoping canyon at the surface or the Hoping basement rise in depth. Even if a few of them locate onto the subduction interface, most of them occur within the upper plate, often at shallow depths. Focal mechanisms within the shallow group indicate either a high-angle backthrust dipping south or a north dipping low-angle thrust [*Font et al.*, 2003; *Font and Lallemand*, 2009]. Together with additional data the authors propose the existence of an active splay fault, probably resulting from the subduction of an oceanic relief and causing the abnormal seismic activity [*Font and Lallemand*, 2009]. Such splay faults, connected onto the subduction plate interface, are able to generate a mega-thrust earthquake such as those known in Nankai

or Sumatra. At the same time, the authors were puzzled by both the shallowness of most events and the fact that no surface evidence of splay fault emergence was observed. They thus questionned the accuracy of earthquake location with a large azimuthal gap in land stations with respect to the offshore events. In order to better constrain the seismic activity in this highly deformed region, two seismic experiments were conducted: one active during which a combined wide-angle and reflection seismic profile was acquired across the Ryukyu arc east of Taiwan, and a passive one consisting of 3-months passive recording of the natural seismicity in the study area (see *Theunissen et al., this issue*).

2. OBS data acquisition and preprocessing

During the RATS-3 (Ryukyu Active Tectonics) cruise in 2009, one combined wide-angle and reflection seismic profile of 300 km length was shot spanning from the Okinawa basin and crossing the Ryukyu subduction system (Figure 1). 24 ocean-bottom seismometers (OBS) were deployed along the profile, at an interval of 14-15 km but it was denser (7-8 km) in the seismically active area in the central part of the profile. These instruments included 19 OBS from the Ifremer (French Research Institute for Exploration of the Sea) pool and 5 instruments from NTOU (National Taiwan Ocean University) [*Auffret et al.*, 2004]. All instruments recorded usable data on all four channels. The RATS experiment was combined with the larger TAIGER onshore-offshore experiment [*Lester et al.*, 2010; *Langston et al.*, 2009; *Kuo-Chen et al.*, 2008].

Pre-processing of the OBS data included calculation of the clock-drift corrections to adjust the clock in each instrument to the GPS base time. Instrument locations were corrected for drift from the deployment position during their descent to the seafloor using the direct water wave arrival. The drift of the instruments never exceeded 200 m. Picking

of the onset of first and secondary arrivals was performed without filtering where possible (mostly between offsets of 0 - 40 km). Further processing of the data to facilitate picking at further offsets included deconvolution, application of a 5 to 15 Hz Butterworth filter and equalization. Data quality along the profile was generally very good with clear arrivals to offsets over 100 km between the ship and the sea-floor instrument (Figure 2 A). Clear Pmp reflections can be identified on most instruments located on the Philippine Sea Plate, in the Ryukyu Arc area and in the Okinawa Trough (Figure 2 B). Mantle velocities could be constrained from turning wave arrivals from the upper mantle on some instruments located in the Okinawa Trough and on the Philippine Sea Plate (Figure 2 C).

3. Multichannel seismic data processing

A coincident reflection seismic line MGL0906-12 was shot by the R/V Marcus Langseth (Figure 3). A total of 3057 shots were fired on the profile by a 6600 in^3 tuned airgun array of the R/V Marcus Langseth. These shots were recorded by a 6.0 km 468 channels solid state seismic streamer. The multi-channel seismic reflection data of MGL0906-12 were processed at the Institute of Oceanography, National Taiwan University, with the ProMAX (Landmark) seismic processing software. The data are of high quality, with an excellent signal to noise ratio, relatively flat spectral content, and a well shaped source signature. As a result, no significant improvement was achieved during source designature and spiking predictive deconvolution, and the profiles presented in this study were processed with no deconvolution. The processing sequence is composed of geometry (including streamer feathering), cdp binning at 12.5 m interval and sorting, band-pass filter (2-16-64-96 Hz), re-sampling from 2 to 4 ms. After velocity analysis, true amplitude recovery was applied, normal move-out, multiple attenuation, time variant band-pass filter (from 2-16-48-64

at sea bottom to 2-16-32-48 Hz 3 s below), inside and out-side mute, stack, and post-stack time variant band-pass filter and Kirchhoff time migration. Two pass of semblance velocity analysis (at 500 then 250 cdp) were performed on 8 cdp super-gathers (full fold of 468 channels), using the velocities of the tomographic inversion of the OBS records as guide function in order to constrain stacking velocities at depth where semblance is poor. Multiple attenuation was achieved with an FK-filter applied to super-gathers of 4 cdps (half fold at 25 m trace interval). Moreover, an additional radon velocity filter (from 25 % below to 50 % above) was applied to the south-western portion of the profile in order to further attenuate multiples that compromise seismic imaging of the subducting PSP underneath the accretionary prism. However in this area, structures are poorly imaged: rough topography, little continuity in the reflectors, and steep dips result in high noise and short lived features on the seismic profile.

4. Tomographic inversion

The tomographic inversion code FAST [*Zelt and Barton*, 1998] was further used to construct a first velocity model. This model also served as an initial guideline to the forward modeling, described hereafter. This non-linear tomographic approach consists in a regularized inversion in which user specified parameters weight the final solution in terms of travel time misfit and model roughness. The method is linearized in that a starting model and iterative convergence scheme are employed. Non linearity is accounted for by calculating new ray paths at each iteration. The method generates smooth models which do not resolve sharp boundaries but steeper velocity gradients instead. The most important structural features are thus resolved in an objective manner, i.e., not user-oriented. Additional information from secondary arrivals and gravity modeling were not

incorporated into the inversion in order to keep the approach objective. In order to perform this tomographic inversion of the first arrivals, 16807 travel-times have been picked in the complete dataset. Each pick has been associated to a picking error between 20 ms and 150 ms depending on the data quality. The tomographic model used a grid of 310 km x 40 km with a 0.5 km grid cell size (Figure 4). For the final model run, 5 different smoothing weights were tested in 10 non-linear iterative steps. The final model predicts a mean travel-time misfit of 156 ms. 97 % of all picks were traced in the model.

5. Forward ray-tracing modelling

The data were modelled using a two-dimensional iterative damped least-squares travel-time inversion from the RAYINVR software [*Zelt and Smith*, 1992]. Modelling was performed using a layer-stripping approach, proceeding from the top of the structure towards the bottom. A two-dimensional iterative damped least-squares inversion of travel times was used [*Zelt and Smith*, 1992]. Upper layers were adjusted to improve the fit of lower layers where not directly constrained by arrivals from within the layer. Lateral velocity changes are included into the model only if required by the data, and layers are only included if reflected arrivals or changes in the velocity gradients were necessary to explain all arrivals. Arrival times of the main sedimentary layers and basement were picked from the reflection seismic data figure (Figure 3). These were converted to depth using the OBS data. The depth and velocities of the crustal layers and the upper mantle were modelled from the OBS data only. The error between the picked arrival time and the predicted time from forward modelling indicates the quality of the model for different phases. The number of picks and RMS traveltime residual for all phases are listed in table 1. Velocity gradients and the phase identification in the velocity model were further

constrained by synthetic seismogram modelling using the finite-difference modelling code from the Seismic Unix package [*Cohen and Stockwell*, 2003; *Stockwell*, 1999].

The final model comprises 7 layers: the water layer, two sedimentary layers, an oceanic crustal layer, two arc crustal layers and the upper mantle layer (Figure 5). Each layer is defined by depth and velocity nodes. Water velocity is a constant 1.5 km/s throughout the model. The seafloor model layer includes depth nodes at a spacing of 1 km and sedimentary layers at a spacing of 2.5 km. A node spacing at the deeper crustal layers of 5 km seemed adequate. The velocities of the two sedimentary layers range from 2.0 - 2.2 km/s and 3.5 - 4.5 km/s in the deeper part of the accretionary prism. Velocities in the Ryukyu arc are 4.5 - 5.5 km/s for the upper layer and 5.5 - 7.0 km/s for the lower layer. The limit between these two layers is not constrained by reflected waves but is required to have two different velocity gradients and allow to obtain a better fit of the refracted waves within the arc crust. Mantle velocities are constrained from 7.8 - 8.2 km/s in the oceanic domain, however in the arc region the mantle velocities are not sampled by the seismic rays.

6. Error analysis

In order to constrain the dependency of the final tomographic model of on the initial model, different model runs were conducted using different initial models. A variety of simple initial models where constructed and the inversion performed (Figure 6). The resulting models are characterized by an equal or lower fit of the data. Models calculated from a horizontal Moho or a Moho dipping towards the northeast lead to nearly identical results (Figures 6 A, B, C, and D). Model using an unrealistic deep Moho at the SW end

of the profile lead to mantle velocities higher than 8.6 km/s (Figures 6 E and F). The shallow layers in the final model do not depend on the initial model.

Checkerboard tests using synthetic data were performed in order to constrain the resolution of the model in different depths using the given experiment geometry. Synthetic models consisting of sinusoidal anomalies were superimposed onto the final velocity model of Figure 3a. The maximum amplitude of the anomalies in the synthetic models is +5% and −5% of the background velocity. Synthetic noisy data with the same source-receiver geometry as in the data set used for the final results have been generated for these models. The result of the inversions after one iteration starting from the reference model of Figure 4 and using the synthetic data set and the differences between the synthetic and inverted models are displayed in Figure 7. Up to a depth of 10-15 km a checkerboard pattern of cells of the size of 10 km x 5 km can be very well resolved (Figure 7 A and B). In the SW part of the model a pattern including cells of the size 20 km x 10 km is well resolved while the amplitude of the cells in the NE part of the model is weaker that the amplitude of the superimposed anomalies (Figure 7 C and D). Even the very deep structures allow the resolution of anomalies of the size 40 km x 15 km (Figures 7 E and F).

Ray coverage of the tomographic and the forward model is generally very good (Figure 5 (B) and 4 (B)). The ray coverage is slightly higher in the forward model resulting mainly from the additional reflected phases which have been modelled. Generally the ray coverage is higher in the region of densest OBS spacing between 50 and 150 km model offset. The fit between predicted arrival times and travel-time picks provides information about the quality of the model, and can be described by the root mean square (rms) error. The final tomographic model is characterised by a rms-error of 134 ms. The root-mean-square

error of the forward model is slightly higher (141 ms) due to the difficulty of picking and modelling the secondary and reflected phases, which are included in the forward model only. The χ^2 is defined as the root-mean-square traveltime misfit between observed and calculated arrivals normalised to the picking uncertainty. The number of picks, the phase number and the rms misfit for the most important phases of the models of the forward model are listed in Table 1.

In order to constrain the velocity gradients of the different layers, synthetic seismograms were calculated and compared to the data sections. The finite difference modeling code from the Seismic Unix package (Cohen and Stockwell, 2003; Stockwell, 1999) was used to calculate synthetic seismograms of a record length of 30 s at a 100 m spacing (Figure 8). The program uses the explicit second order differencing method for modeling the acoustic wave equation. The input velocity model was calculated from sampling the forward velocity model at a lateral 50 m interval and 10 m interval in depth. In order to avoid grid dispersion, the peak frequency of the Ricker wavelet source signal is calculated to be equal to the lowest velocity of the medium divided by the grid points per wavelength multiplied by 10. In this case the source wavelet is centered at 8 Hz, similar to the signal from the airgun array used during the cruise. The boundary conditions were set to be absorbing at the sides and bottom of the model and free at the surface.

The region between sedimentary wedge, arc crust and oceanic plate is not imaged clearly by the MCS data, and information regarding its geometry can therefore only be gained from both inversion and forward modeling of the wide-angle seismic data. In order to avoid the introduction of unconstrained features, several backstop geometries were tested (Figure 9). Firstly, a simple geometry using a smooth inclination as has been interpreted

by *Wang et al.* [2001] with less dense OBS network on the seafloor. In this case, the phases reflected from the continental crust arrive too early and some refracted waves does not fit the data well. Thus, the resulting model is characterised by a higher RMS error and a lower percentage of picks which could be successfully reached by rays than in the final velocity model. Secondly, as the inverse model shows a very steep inclination of the isovelocity contours in this region, a near-vertical position of the backstop, as already proposed by *Font et al.* [2001], was tested. Although the rms-error is as high as in the previous model, the trend of the refracted waves passing through the backstop and those of the reflected waves on the sides better fit the picked arrivals. Thus, our data support the existence of a sharp backstop. Refinement of this model resulted in our final velocity model which is characterised by an abrupt nearly vertical backstop including low velocities at the front end of the backstop. The rms-error of this model is 142 ms and 95 % of the picks can be explained.

7. Comparison with reflection seismic data

The wide-angle seismic models converted to two-way travel-time show good agreement with the reflection seismic section (Figures 10). The most prominent sedimentary reflectors were digitised from the reflection seismic section and set in the forward modelling with slight adjustments where necessary to fit the OBS data. However, only sedimentary reflectors discernible in the OBS data and therefore necessary for the modelling were included to avoid over-parametrization of the inversion. Velocities of these main sedimentary layers were constrained by wide-angle seismic data, but some additional layering is imaged by the reflection seismics. Depth of the acoustic basement is in very good agreement along the complete model. Reflections from the Moho are not discernible in the MCS section.

Part of the profile, including the accretionary prism and backstop, were depth-converted using the stacking velocities in the shallow layers and velocities from the tomographic model for deeper layers. Comparison of the velocity model with the reflection seismic data is in good agreement for both models, but no reflections from the backstop can be traced in the MCS section. However the nearly vertical change in velocities can be correlated with a change in reflectivity pattern from highly reflective northeast of the backstop to nearly transparent southwest of it, confirming the existence of an heterogeneity across the boundary.

8. Results and discussion

The tomographic inversion of wide-angle seismic data from the Ryukyu subduction zone offshore Taiwan allows to image the accretionary prism and the subducted slab up to a depth of 25 km (Figure 4, 5 and 11). The thickness of the sedimentary layers is between 2 and 3 km on the oceanic plate and only 1.5 to 2 km in the northwestern end of the

Profile in the Okinawa Trough. *Klingelhoefer et al.* [2005] suggest that the high velocity contrast found between the sedimentary layers and the accoustic basement might be due to the inclusion of some backarc volcanism or arc relics emplaced during formation of older backarc basins since early Tertiary. The sedimentary layer overlying the Huatung Basin oceanic crust is about 2 to 3 km thick approaching the trench. The seismic velocities are well constrained for these layers due to the close instrument spacing and reach a maximum of 5.5 km/s for deeper layers, where they might represent the top of the basalt layer.

Velocities within the oceanic crust in the tomographic and forward model are comparable. The resulting oceanic crustal thickness of about 5-6 km is therefore slightly thinner than normal oceanic crust [*White et al.*, 1992] (Figure 12). Also velocities from the tomographic inversion are lower than normal oceanic crust. These results are in good agreement with crustal thickness from expanding spread profiles (ESP) found by Murauchi et al., 1973, who find a mean crustal thickness in the Philippine Sea of 5.60 km and *Louden* [1980] who determined a crustal thickness between 3 and 6 km from equally from ESP. This is also consistent with the result of Taicrust line 23 modelled by [*McIntosh et al.*, 2005], who clearly defined relatively thin, oceanic crust in the Huatung Basin. The subduction angle of the subducting oceanic slab increases at a model distance around 70 km and 110 km, possibly due to forearc loading and compression. *Wang et al.* [2001], after processing of TAICRUST line EW-01 also showed a break in the subduction angle of the slab right beneath the forearc basin (equivalent of a distance of 95 km in our model) that he attributed to forearc compression and possible slab break-off. Differences between the earlier models and the one shown in this study can be explained by the denser OBS

network deployed in our study and the more modern reflection seismic data acquisition techniques used during the ACTS cruise.

A backstop is identifiable in both tomographic and forward ray-tracing model and characterized by an abrupt lateral velocity change in the tomographic model and a nearly vertical boundary in the forward model. Its location corresponds to a change in the reflectivity pattern of the MCS data (Figure 10). However, the resolution of this area is medium only and no reflections from the vertical boundary were used in the forward model. The TAICRUST wide-angle seismic line EW9509-1, located close to our profile [*Wang et al.*, 2001, 2004] reveals similar sedimentary thickness at the accretionary wedge, however the inclination of the backstop dips regularly toward the trench down to the top of the slab on the interpreted TAICRUST profile (Figure 1). One explanation of this difference is that the two profiles cross a 3D irregular backstop at different angles (Figure ?? ou 1), a feature which might result from the oblique subduction. Another explanation being that the toe of the backstop was not well resolved with the TAICRUST data. Such vertical termination of the backstop has been already observed in the central Chile margin and it has been interpreted by the authors as the consequence of strong tectonic erosion [*Contreras-Reyes et al.*, 2010]. In the forward modeling, a low velocity zone was introduced a low velocity zone to better fit the model. As no reflected waves from this feature can be distinguished in the record sections, its geometry is not well constrained. This kind of structure is very difficult to image as it is deep and rays pass away off a low velocity zone.

Crustal thickness at the Ryukyu Arc is about 25 km and the arc has been modelled using two layers with velocities between 4.50 to 5.50 and 5.50 to 7.00 km/s. The upper

328 layer has a thickness of about 4.4 km from the Okinawa through to the arc and then
329 pinching out at the backstop. The second layer has a maximum thickness of about 20 km,
330 thinning towards the Okinawa Trough and equally pinching out at the backstop. Moho
331 depth in the Okinawa Trough itself is not constrained by our dataset further than to 200
332 km model distance. *Klingelhoefer et al.* [2005] find a Moho depth around 12 km in the
333 central part of the Okinawa Trough. The Moho depth found by *Lee et al.* [1980] in the
334 Okinawa trough is slightly deeper, a fact which might be explained by the location of the
335 profile slightly further east.

336 The mantle underlying the oceanic crust is characterised by seismic velocities of 7.80
337 km/s slightly lower than normal mantle velocities. No rays turning in the mantle under-
338 lying the arc could be identified in the data sections. Here, the Moho depth was modelled
339 using PmP reflections. A similar reduction in upper oceanic mantle velocities was ob-
340 served offshore Costa Rica over the flexurally faulted portion of the oceanic Cocos plate
341 before it enters the Middle America trench and interpreted as being due to serpentiniza-
342 tion of the uppermost mantle [*Grevemeyer et al.*, 2005] through faults generated by the
343 flexure and imaged on seismic reflection data [*Ranero et al.*, 2003]. Similar low velocities
344 are found underneath the subducting oceanic plate in the Sumatra subduction zone [*Klin-*
345 *gelhoefer et al.*, 2010]. In all three environments, the oceanic crust is thinner than usual
346 and might thus be fractured more readily and therefore may permit a higher degree of
347 serpentinization in the upper mantle than thick oceanic crust. Furthermore, the basement
348 of the Huatung basin is characterized by N-S trending ridges and troughs that parallel
349 the Gagua Ridge and were interpreted as satellite transform faults, creating additional
350 fractures [*Deschamps et al.*, 1998].

9. Conclusions

Velocity modelling of wide-angle seismic data of a profile located over the whole trench-arc-backarc system, from the Ryukyu trench to the Okinawa back-arc trough allows to image the subducting slab down to a depth of up to 25 km. Based on this velocity model we propose that :

1) The sedimentary thickness on the oceanic plate is about 2-3 km,

2) The thickness of the oceanic crust is about 5-6 km, slightly thinner than normal oceanic crust,

3) Both the tomographic inversion of first arrivals and the forward model reveal a backstop characterised by a very steep inclination. Although this region of the model is not highly constrained and no reflections from the backstop can be identified in multi-channel seismic data, it produces the lowest error of several geometries tested. Low velocities are observed at the base of the backstop in the tomographic inversion and are confirmed by forward modeling. This could be the sign of active tectonic erosion,

4) Our forward model indicates a deflection of the subducting PSP beneath the forearc buttress that may reveal compression and/or overloading,

5) The upper mantle material underlying the oceanic plate is characterised by relatively low seismic velocities which might be due to the partial serpentinisation of the mantle peridotites by water passing through faults in the oceanic plate. The faults might be generated by the bending of the subducting plate before subducting, but also by an early fabric.

Acknowledgments.

We would like to thank all colleagues from the TAIGER project who made it possible to acquire this profile during their experiment. We also would like to thank the captain and the crew of the R/V Yun-Ying 2 and the R/V Marcus Langseth. Acquisition and processing of the data were funded by the Agence Nationale de la Recherche and Ifremer. Many thanks to Anne Delplanque for help with the figures. The GMT [*Wessel and Smith*, 1995] and Seismic Unix software package [*Stockwell*, 1999] were used in the preparation of this paper.

References

Auffret, Y., P. Pelleau, F. Klingelhoefer, L. Gï£¡li, J. Crozon, J.-Y. Lin, and J.-C. Sibuet, Microbs : a new generation of bottom seismometer., *First Break*, pp. 41–47, 2004.

Chemenda, A., R. K. Yang, C. H. Hsieh, and A. Groholski, Evolutionary model for the taiwan collision based on physical modeling, *Tectonophysics, 274*, pp. 253–274, 1997.

Chen, R. Y., H. Kao, W. T. Liang, T. C. Shin, Y. B. Tsai, and B. S. Huang, Three-dimesional pattern of seismic deformation in the taiwan region with special implication from the 1999 chi-chi earthquake sequence, *Tectonophysics, 446*, pp. 140–151, 2009.

Cohen, J. K., and J. W. Stockwell, Seismic Unix Release 37: a free package for seismic research and processing, *Center for Wave Phenomena, Colorado School of Mines.*, 2003.

Contreras-Reyes, E., E. R. Flueh, and I. Grevemeyer, Tectonic control on sediment accretion and subduction off central chile : Implications for coseismic rupture processes of the 1960 and 2010 megathrust earthquakes, *Tectonics, 29, TC6018, doi :10.1029/2010TC002734*, 2010.

Deschamps, A., S. Lallemand, and J. Y. Collot, A detailed study of the Gagua Ridge: A fracture zone uplifted during a plate reorganisation in the Mid-Eocene , *Marine*

Geophys. Research, *20*, 403–423, 1998.

Font, Y., and S. Lallemand, Subducting oceanic high causes compressional faulting in southernmost Ryukyu forearc as revealed by hypocentral determinations of earthquakes and reflection/refraction seismic data, *Tectonophysics, 466 (3-4)*, pp. 255–267, 2009.

Font, Y., S.-C. Liu, P. SchnÃijrle, and S. Lallemand, Constraints on backstop geometry from the southwest Ryukyu subduction based on reflection seismic data, *Tectonophysics*, *333*, 135–158, 2001.

Font, Y., H. Kao, C.-S. Liu, and L.-Y. Chiao, A comprehensive 3D seismic velocity model for the eastern Taiwan-southernmost Ryukyu regions, *Terr. Atm. Oc. Sci., 14*, pp. 159–182, 2003.

Grevemeyer, I., N. Kaul, J. L. Diaz-Naveas, H. W. Villinger, C. R. Ranero, and C. Reichert, Heat flow and bending-related faulting at subduction trenches: Case studies offshore of Nicaragua and Central Chile, *Earth Planet. Sci. Lett., 236*, pp. 238–248, 2005.

Hagen, R. A., F. K. Duennebier, and V. Hsu, A seismic refraction study of the crustal structure in the active seismic zone east of Taiwan., *J. Geophys. Res., 93 (B5)*, pp. 4785–4796, 1988.

Hetland, E. A., and F. T. Wu, Deformation of the Philippine Sea Plate under the Coastal Range, Taiwan: Results from an offshore-onshore seismic experiment, *TAO, 9*, pp. 363–378, 1998.

Hsu, S.-K., and J.-C. Sibuet, Earthquake off japan could generate strong tsunami, *EOS, 86(17)*, pp. 169–170, 2005.

Klingelhoefer, F., R. A. Edwards, R. W. Hobbs, and R. W. England, Crustal structure of the NE-Rockall Trough from wide-angle seismic data modelling, *J. Geophys. Res., 110*, p. B11105, 2005.

Klingelhoefer, F., M.-A. Gutscher, S. Ladage, J.-X. Dessa, D. Graindorge, D. F. C. Andre, H. Permana, T. Yudistira, and A. Chauhan, The limits of the seismogenic zone in the epicentral region of the 26 dec. 2004 great Sumatra-Andaman earthquake: results from a seismic refraction and wide-angle reflection surveys and thermal modeling, *J. Geophys. Res. 115, B01304, doi:10.1029/2009JB006569, 2010*, pp. 1–23, 2010.

Kuo-Chen, H., F. T. Wu, Y. Nakamura, C. Lee, and K. MacIntosh, Relocation of earthquakes and tectonics of offshore Taiwan with the addition of TAIGER BBOBS, *Eos, Transactions, American Geophysical Union, 89 (53)*, pp. T31C–2023, 2008.

Langston, C. A., W. H. K. Lee, C.-J. Lin, and C.-C. Liu, Seismic-wave strain, rotation, and gradiometry for the 4 march 2008 taiger explosions, *Bull. Seis. Soc. Am., 99 (2B)*, pp. 1287–1301, 2009.

Lee, C.-S., G. G. Shor, L. D. Bibee, R. S. Lu, and T. W. C. Hilde, Okinawa Trough: Origin as backarc basin, *Mar. Geology, 35*, pp. 219–241, 1980.

Lester, W. R., K. McIntosh, and H. van Avendonk, Seismic velocity structure of the Eurasian Continental Margin in the Northern South China Sea from wide-angle obs data, *Proceedings from the 2010 AGU Western Pacific Geophysics Meeting*, pp. 22–25, 2010.

Leyden, R., M. Ewing, and S. Murauchi, Sonobuoy refraction measurements in East China Sea, *Am. Assoc. Pet. Geol. Bull. 57 (12)*, pp. 2396–2403, 1973.

438 Louden, K., The crustal and lithospheric thicknesses of the Philippine Sea as compared
439 to the Pacific, *Earth Planet. Sci. Lett., 50*, pp. 275–288, 1980.
440 Ludwig, W. J., N. Kumar, and R. E. Houtz, Profiler-sonobuoy measurements in the South
441 China Sea Basin, *J. Geophys. Res., 84(B7)*, pp. 3505–3518, 1979.
442 McIntosh, K., and Y. Nakamura, Crustal structure beneath the nanao Forearc Basin from
443 TAICRUST MCS/OBS Line 14, *TAO, 9*, pp. 345–362, 1998.
444 McIntosh, K., Y. Nakamura, T.-K. Wang, R.-C. Shih, A. Chen, and C.-S. Liu, Crustal-
445 scale seismic profiles across Taiwan and the western Pilippine Sea, *Tectonophys., 401*,
446 pp. 23–54, 2005.
447 Murauchi, S., N. Den, S. Asano, H. Hotta, T. Yoshii, T. Asanuma, K. Hagiwara,
448 K. Ichikawa, T. Sato, W. J. Ludwig, J. I. Ewing, N. T. Edgar, and R. E. Houtz,
449 Crustal structure of the Philippine Sea, *J. Geophys. Res., 73*, pp. 3143–3171, 1968.
450 Ranero, C. R., J. P. Morgan, K. McIntosh, and C. Reichert, Bending-related faulting and
451 mantle serpentinization at the Middle America Trench, *Nature*, pp. 367–373, 2003.
452 Seno, T., S. Stein, and A. Gripp, A model for the motion of the philippine sea plate
453 consistent with NUVEL-1 and geological data, *J. Geophys. Research*, *98*, 17,941–17,948,
454 1993.
455 Stockwell, J. W., The cwp/su: Seismic un*x package, *Computers and Geosciences*, 1999.
456 Theunissen, T., Y. Font, S.Lallemand, and W. T. Liang, The largest instrumentally
457 recorded earthquake in Taiwan : revised location and magnitude, and tectonic sig-
458 nificance of the 1920 event, *Geophys. J. Int., doi: 10.1111/j.1365-246X.2010.04813.x*,
459 *183*, 1119–1133, 2010.

460 Wang, T. K., and C.-H. Chiang, Imaging of arc-arc collision in the Ryukyu forearc region
461 offshore hualien from TAICRUST OBS Line 16, *TAO, 3*, pp. 329–344, 1998.
462 Wang, T. K., K. Mcintosh, Y. Nakamura, C.-S. Liu, and H.-W. Chen, Velocity-interface
463 structure of the southwestern Ryukyu subduction zone from EW9509-1 OBS/MCS data,
464 *Mar. Geophys. Res., 22*, pp. 265–287, 2001.
465 Wang, T. K., S.-F. Lin, C.-S. Liu, and C.-S. Wang, Crustal structure of the southernmost
466 Ryukyu subduction zone: OBS, MCS and gravity modelling, *Geophys. J. Int., 157*, pp.
467 147–163, 2004.
468 Wessel, P., and W. H. F. Smith, A new version of the Generic Mapping Tool (GMT),
469 *EOS, Trans. Am. Geophys. Un., 76*, p. 329, 1995.
470 White, R. S., D. McKenzie, and R. O'Nions, Oceanic crustal thickness from seismic mea-
471 surements and rare earth element inversions, *J. Geophys. Res. 97*, pp. 19,683–19,715,
472 1992.
473 Yang, Y.-S., and T. K. Wang, Crustal velocity variation of the Philippine Sea Plate from
474 TAICRUST OBS/MCS Line 23, *TAO. 9*, pp. 379–393, 1998.
475 Yeh, Y. H., R. C. Shih, C. H. Lin, C. C. Liu, H. Y. Yen, B. S. Huang, C. S. Liu, P. Z.
476 Chen, C. S. Huang, C. J. Wu, and F. T. Wu, Onshore/offshore wide-angle deep seismic
477 profiling in Taiwan, *TAO. 9*, pp. 301–316, 1998.
478 Yu, S. B., H. Y. Chen, and L. Kuo, Velocity field of GPS stations in the Taiwan area,
479 *Tectonophysics 274(1-3)*, pp. 41–59, 1997.
480 Zelt, C., and P. Barton, Three-dimensional seismic refraction tomography : a comparison
481 of two methods applied to data from the Faeroe Basin, *J. Geophys. Research*, *103*,
482 7187–7210, 1998.

Zelt, C. A., and R. B. Smith, Seismic travel time inversion for 2-d crustal velocity structure, *Geophys. J. Int. 108*, pp. 16–31, 1992.

10. Figure Captions

Figure 1: Bathymetry of the study region offshore Taiwan with contours every 1000 m. Bold line shows the wide-angle seismic profile and major physiographic features are annotated. Inverted triangles mark OBS positions of the RATS-3 profile and circles position of OBS from the passive experiment. Dashed lines labelled EW refer to the wide-angle profiles acquired during the TAICRUST cruise onboard R/V M. Erwing in 1995. Inset shows regional setting.

Figure 2: Examples of the wide-angle seismic data. Processing included deconvolution, application of a 5–15 Hz Butterworth filter and equalization. (A) OBS 03 located in the Okinawa Trough (B) OBS 17 located on the accretionary wedge (C) OBS 23 located on the Philippine Sea Plate.

Figure 3: (A) Multichannel seismic data. (B) Multichannel seismic data with overlain layer boundaries from velocity modelling.

Figure 4: (A) Result of the tomographic inversion of first arrivals on a 0.5 x 0.5 km grid. Model boundaries from the forward modelling are overlain. OBS locations are indicated by red circles. (B) Ray coverage of the velocity model (0.5 x 0.5 km grid).

Figure 5: (A) Final velocity model from forward modelling including the model boundaries (solid lines) and isovelocity contours every 0.50 km/s. OBS locations are indicated by red circles. Areas unconstrained by raytracing modelling are shaded. (B) Ray coverage of the velocity model (0.5 x 0.5 km grid).

Figure 6: Results fromt the test of different starting models. (A) Starting model including a flat Moho at 12 km depth. (B) Resulting model after 5 iterations. (C) Starting model including a Moho dipping to the NE. (D) Resulting model after 5 iterations. (E) Starting model including a Moho dipping to the SW. (F) Resulting model after 5 iterations.

Figure 7: Results of the checkerboard test. (A) synthetic model including anomalies of the size 10 km x 5 km. (B) Resulting model after one iteration. (C) synthetic model including anomalies of the size 20 km x 10 km. (D) Resulting model after one iteration. (E) synthetic model including anomalies of the size 40 km x 15 km. (F) Resulting model after one iteration.

Figure 8: (a) Bandpass filtered (3-5 Hz, 24-36 Hz) vertical geophone data section from OBS 17. The data are displayed with a gain proportional to source-receiver offset and are reduced at a velocity of 8 km/s. PmP (reflection from the Moho), and Pn (turning waves fromt he upper mantle) are annotated (b) Synthetic seismograms calculated from the velocity model for the same station using the finite-difference modelling code from the Seismic Unix package (Cohen, 2003; Stockwell, 1999). The synthetic seismograms are calculated every 100 m with a source frequency centred around 5 Hz.

Figure 9: (a) Different geometries of the backstop. (a) model with a smoothly decling backstop (b) model with a steep backstop (c) final velocity model

Figure 10: Comparison of the velocity models with multi-channel seismic data. (A) MCS data underlain by the tomographic velocity model. Red dots mark position of the OBS. (B) MCS data underlain by the forward velocity model. Red dots mark position of the OBS.

526 **Figure 11**: Interpreted geological cross section based on the forward and tomographic
527 velocity model.

528 **Figure 12**: Velocity-depth relationship for the oceanic crust at -50, -25, 0 25 and 50 km
529 model distance. Black lines are from the forward and dashed lines from the tomographic
530 model. Grey-shaded area is from *White et al.* [1992] for normal oceanic crust.

531 **Figure 11**: Bathymetry of the study area. Location of the Profiles RATS-3 and
532 TAICRUST EW9509-1 are marked by black lines and position of the OBS by inverted
533 triangles.

Phase		No of picks	RMS traveltime residual	chi-squared
Water	1	1785	0.040	0.163
Sediments 1	2	107	0.101	1.040
Sediments 1 reflection	3	378	0.131	1.721
Sediments 2	4	1708	0.182	3.303
Sediments 2 reflection	5	1717	0.123	1.515
Arc upper crust	6	3831	0.130	1.685
Arc Moho	7	1873	0.182	3.296
Oceanic crust	8	3187	0.155	2.402
Oceanic Moho	9	320	0.150	2.258
Oceanic mantle	11	2843	0.133	1.757
Arc lower crust	12	7863	0.143	2.059
All Phases		25612	0.142	2.009

Table 1. Traveltime residuals and chi squared error for all phases and the complete model.

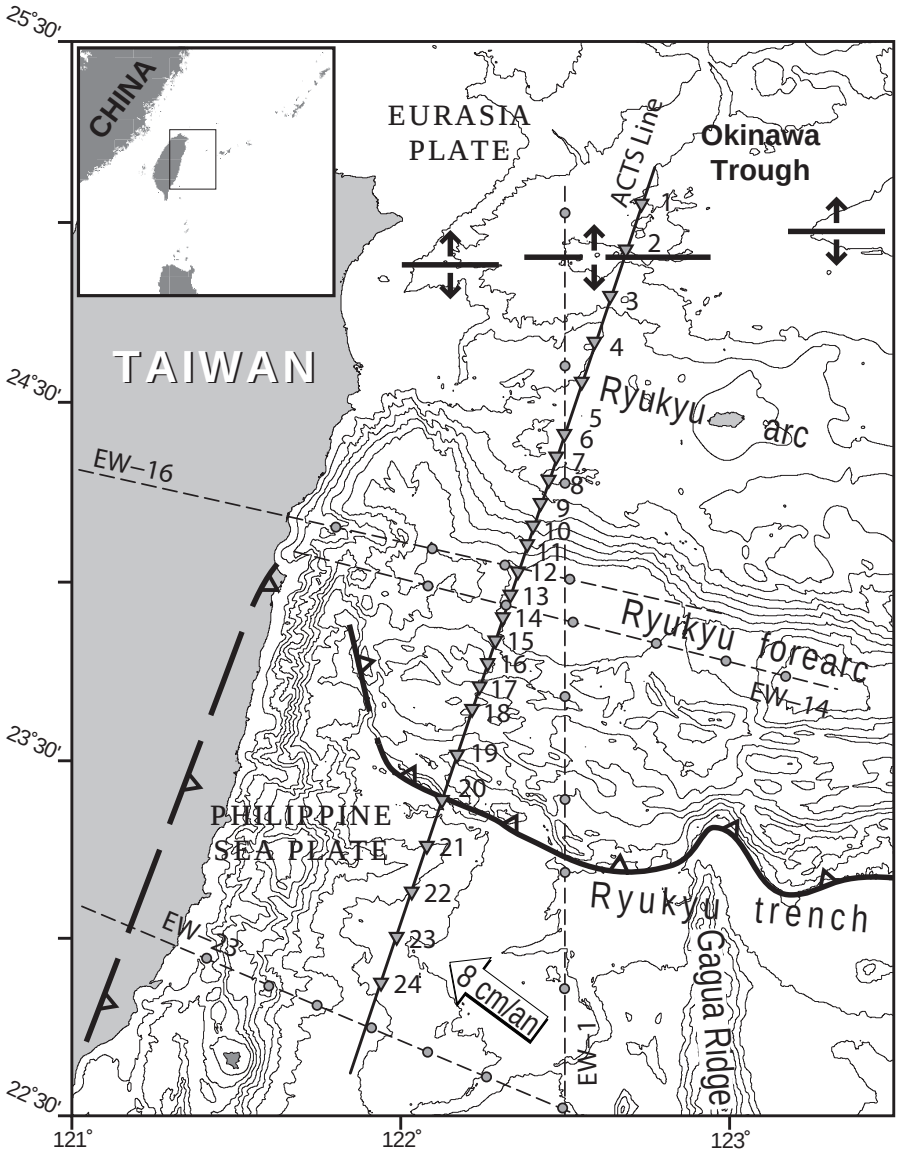
CHINA
EURASIA PLATE
ACTS Line
Okinawa Trough
TAIWAN
Ryukyu arc
EW–16
Ryukyu forearc
EW–14
PHILIPPINE SEA PLATE
Ryukyu trench
Gagua Ridge
EW–23
EW–1
8 cm/an
25°30′
24°30′
23°30′
22°30′
121°
122°
123°

Figure 1.

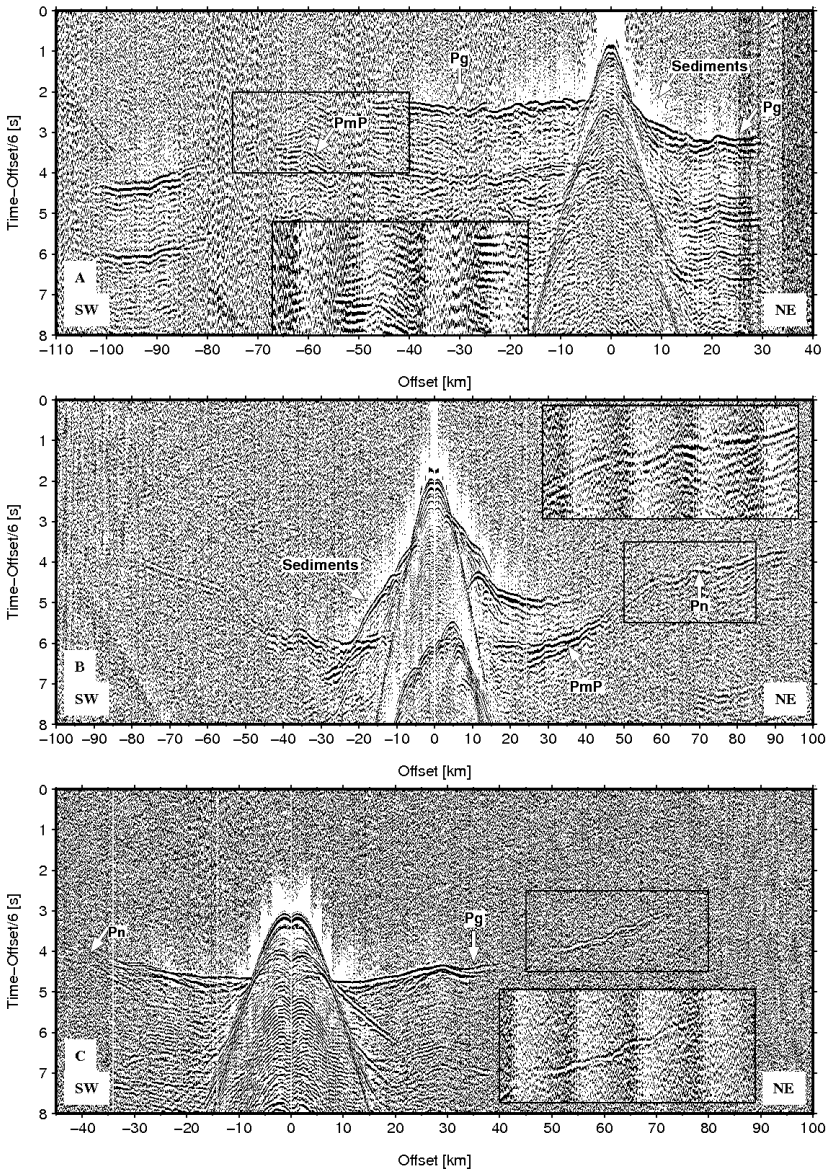
Time–Offset/6 [s]
Offset [km]
Pg
Sediments
Pg
PmP
A
SW
NE
Sediments
Pn
B
SW
PmP
NE
Pn
Pg
C
SW
NE

Figure 2.

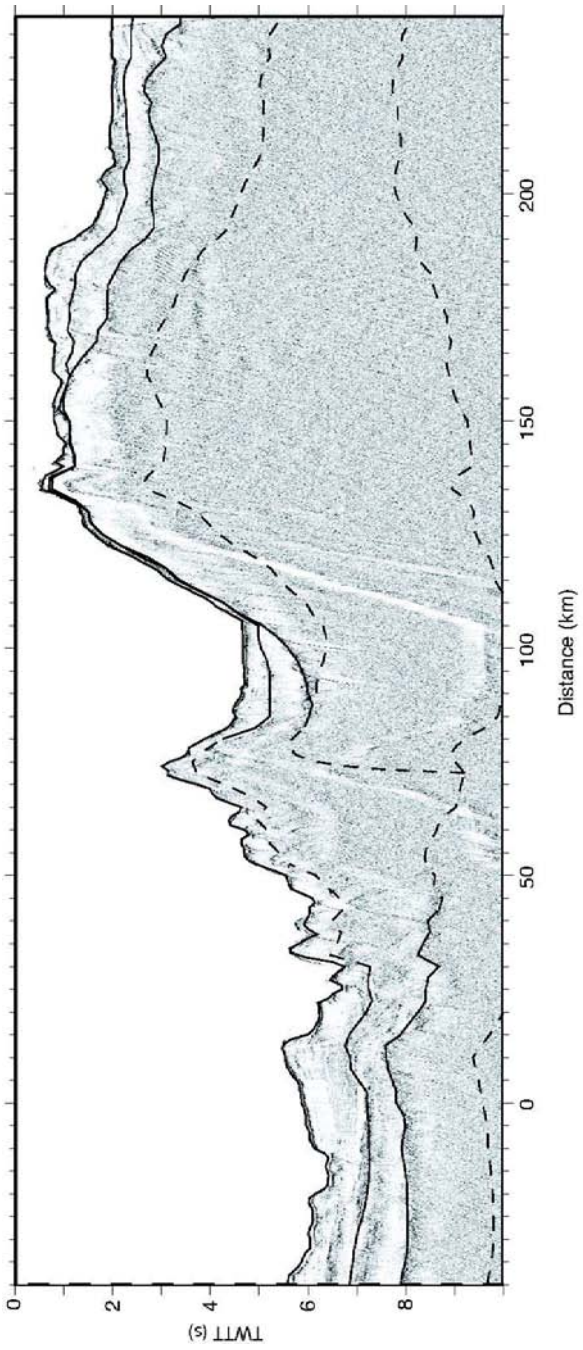

Figure 3.

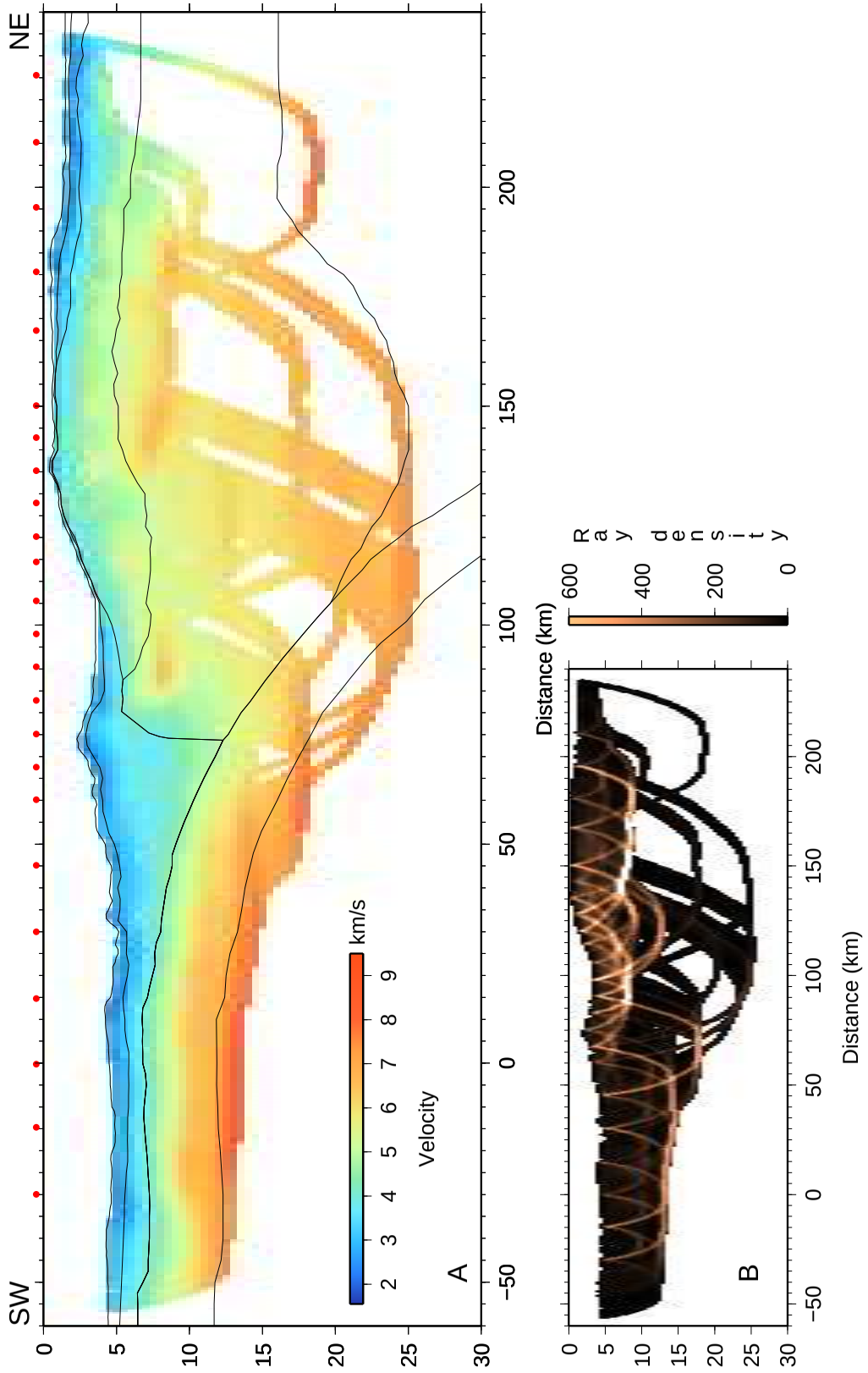

Figure 4.

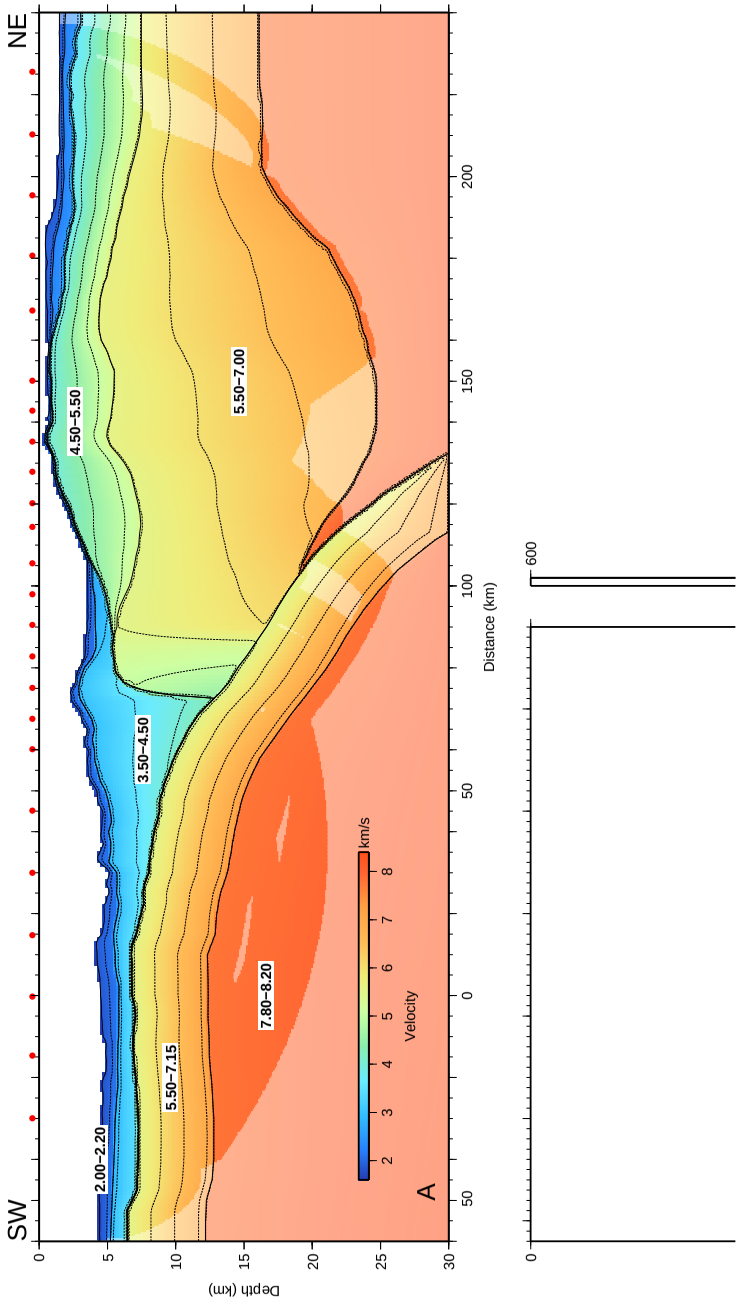
NE
SW
2.00–2.20
3.50–4.50
4.50–5.50
5.50–7.00
5.50–7.15
7.80–8.20
Velocity
km/s
A
Depth (km)
Distance (km)
600

Figure 5.

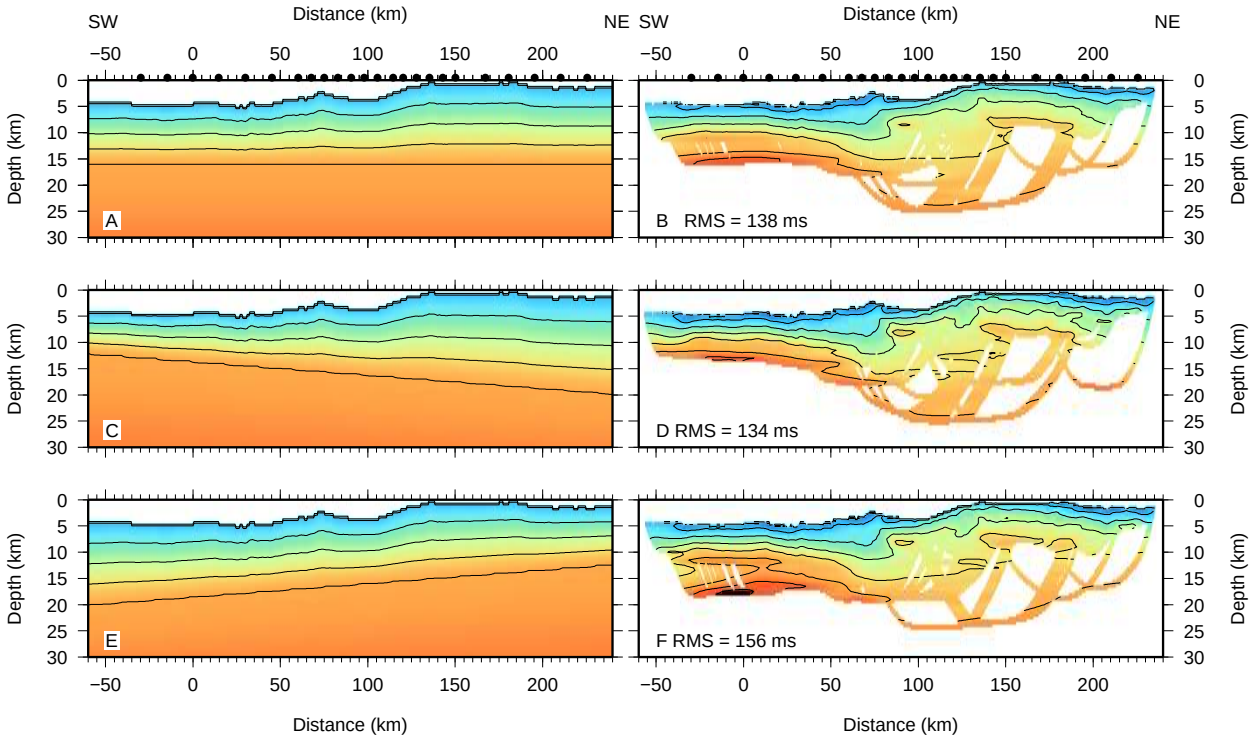
SW
Distance (km)
NE
SW
Distance (km)
NE
−50
0
50
100
150
200
Depth (km)
0
5
10
15
20
25
30
A
B RMS = 138 ms
C
D RMS = 134 ms
E
F RMS = 156 ms

Figure 6.

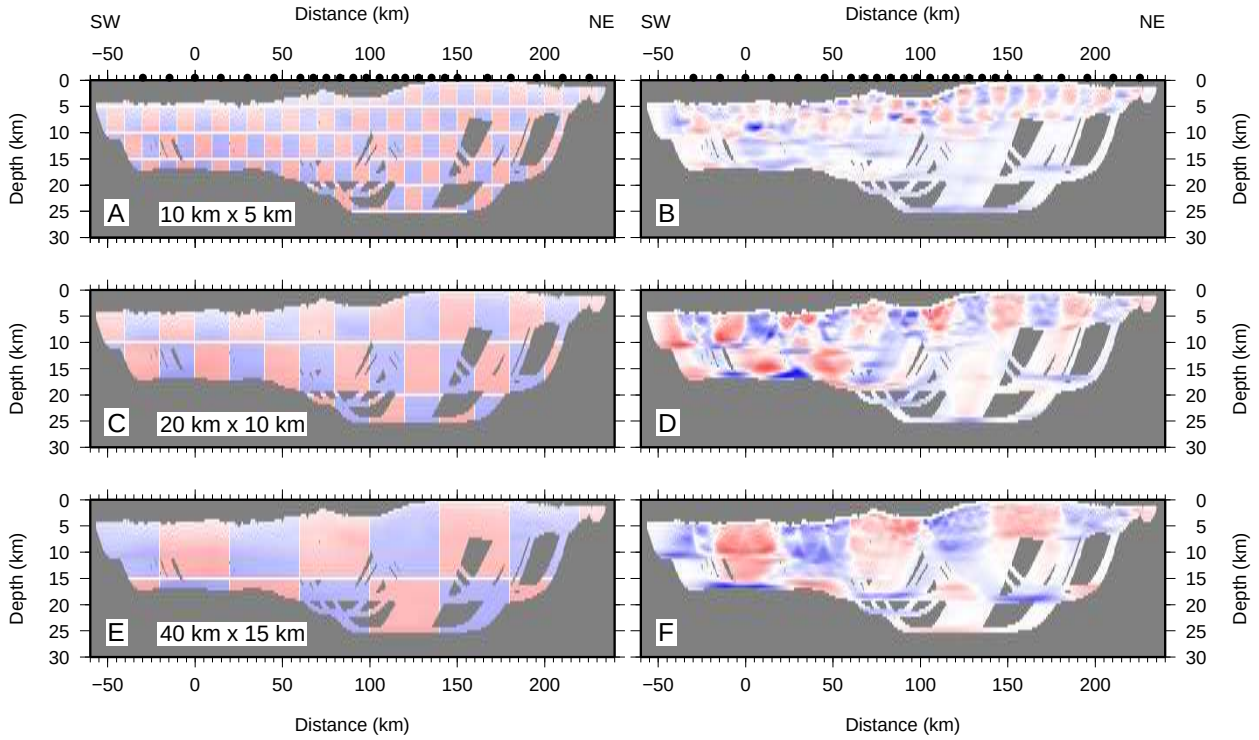
SW
Distance (km)
NE
−50
0
50
100
150
200
Depth (km)
0
5
10
15
20
25
30
A
10 km x 5 km
B
C
20 km x 10 km
D
E
40 km x 15 km
F

Figure 7.

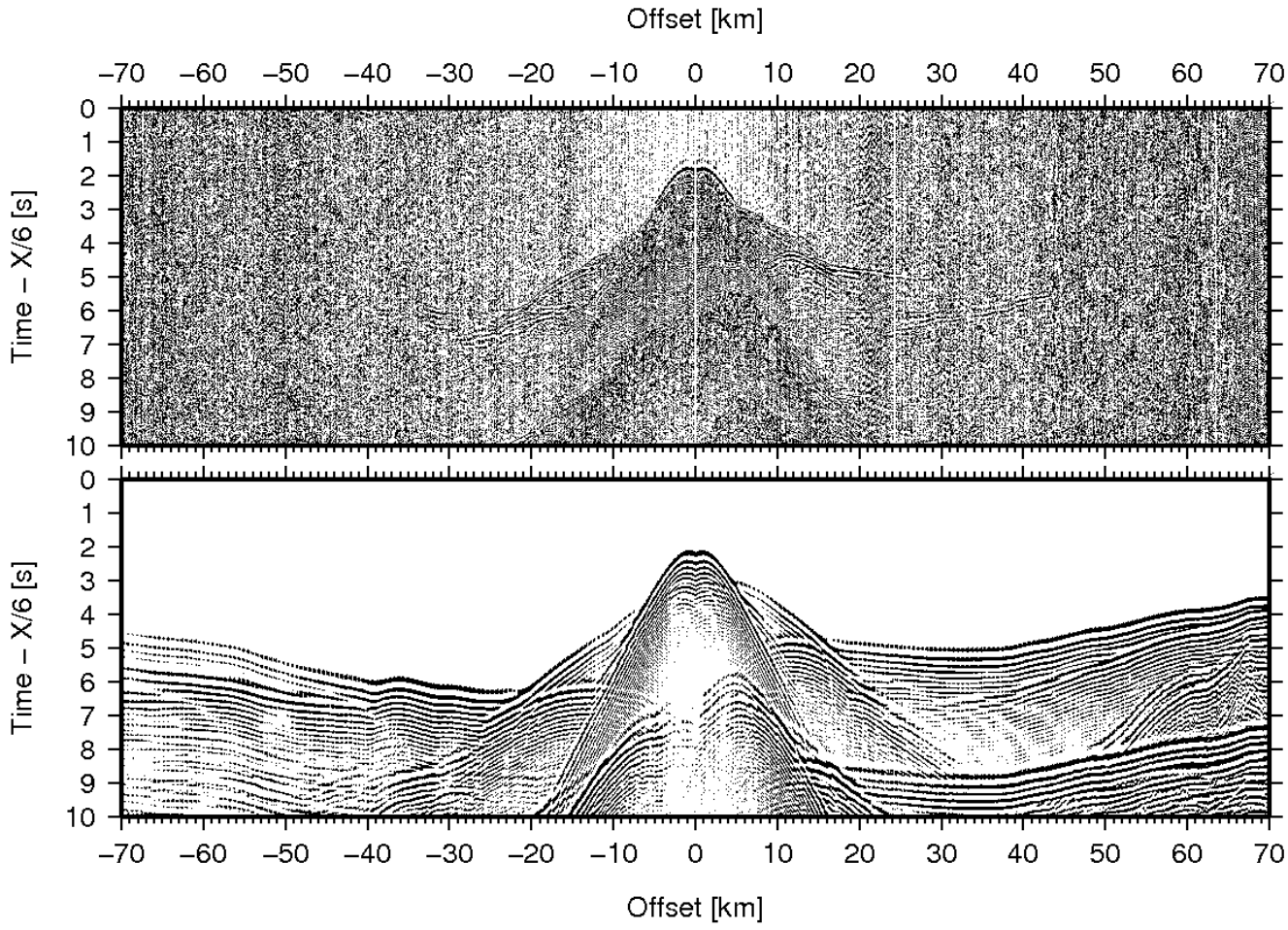
Offset [km]
−70 −60 −50 −40 −30 −20 −10 0 10 20 30 40 50 60 70
Time – X/6 [s]
0 1 2 3 4 5 6 7 8 9 10
Time – X/6 [s]
0 1 2 3 4 5 6 7 8 9 10
−70 −60 −50 −40 −30 −20 −10 0 10 20 30 40 50 60 70
Offset [km]

Figure 8.

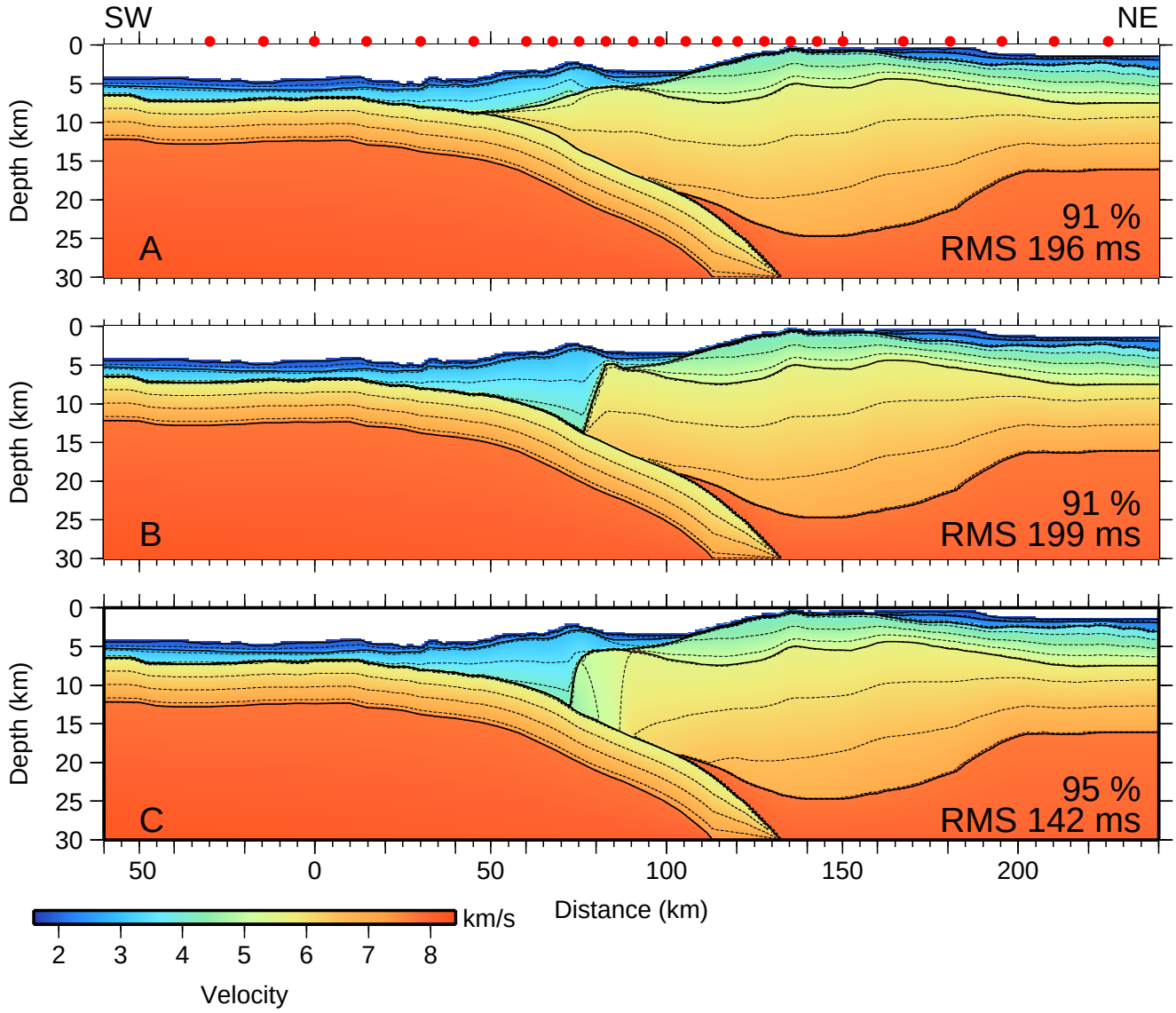
SW
NE
Depth (km)
A
91 %
RMS 196 ms
B
91 %
RMS 199 ms
C
95 %
RMS 142 ms
Distance (km)
km/s
Velocity

Figure 9.

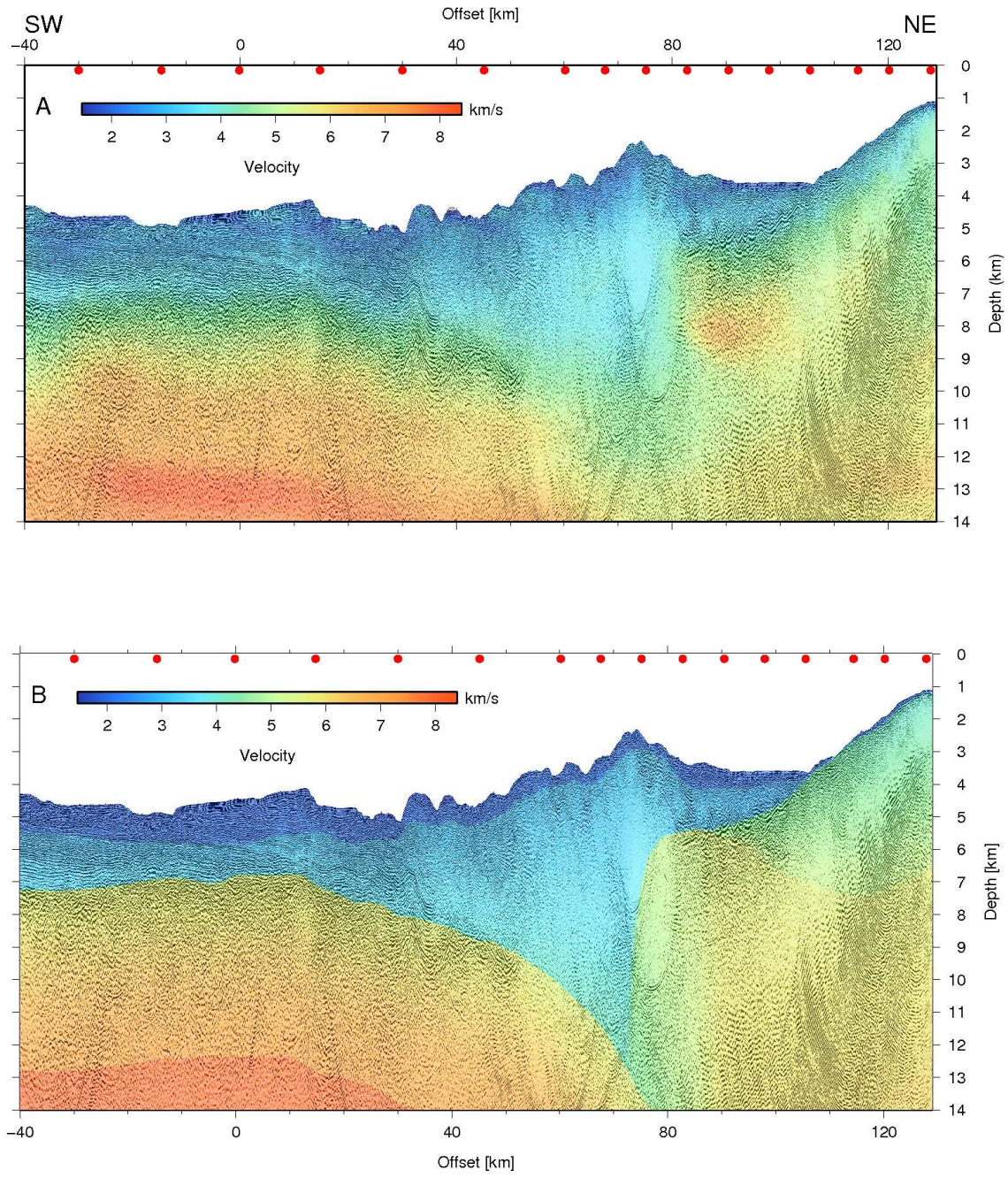
SW
NE
Offset [km]
−40
0
40
80
120
A
km/s
2
3
4
5
6
7
8
Velocity
Depth (km)
0
1
2
3
4
5
6
7
8
9
10
11
12
13
14
B
km/s
2
3
4
5
6
7
8
Velocity
Depth [km]
−40
0
40
80
120
Offset [km]

Figure 10.

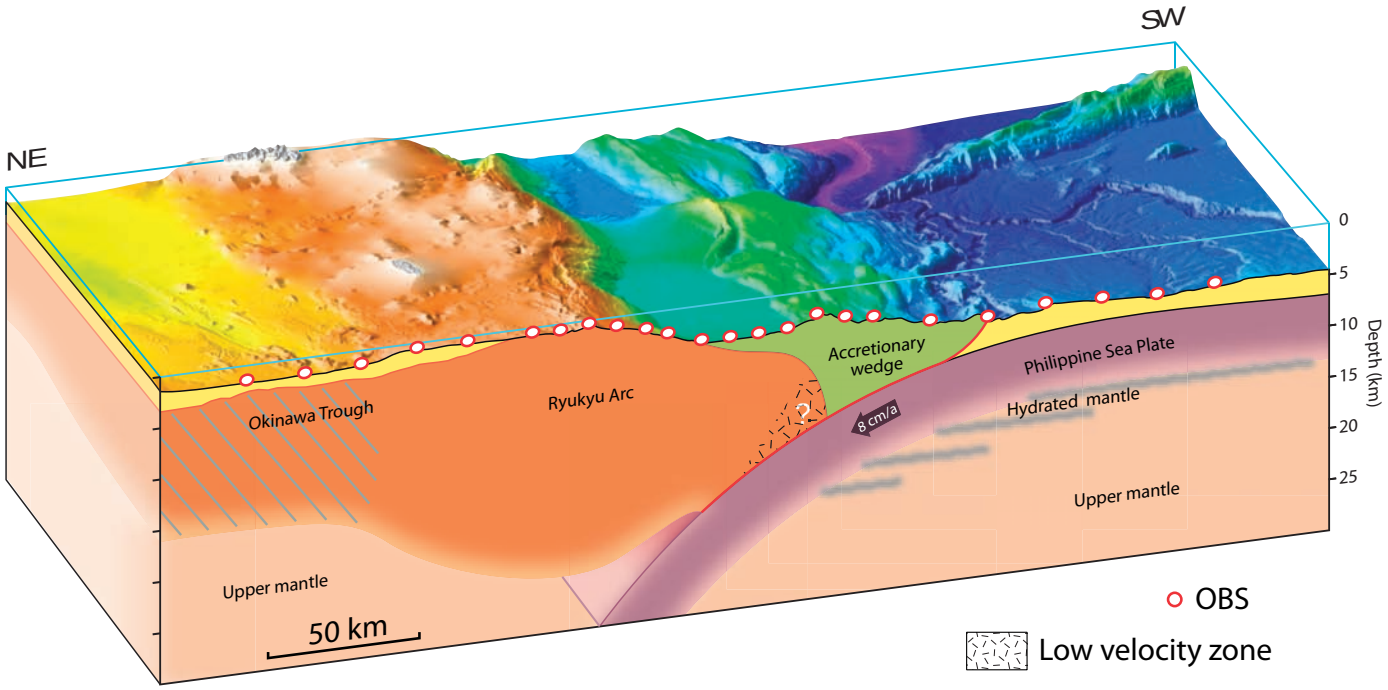
SW
NE
0
5
10
15
20
25
Depth (km)
Okinawa Trough
Ryukyu Arc
Accretionary wedge
8 cm/a
Philippine Sea Plate
Hydrated mantle
Upper mantle
Upper mantle
50 km
OBS
Low velocity zone

Figure 11.

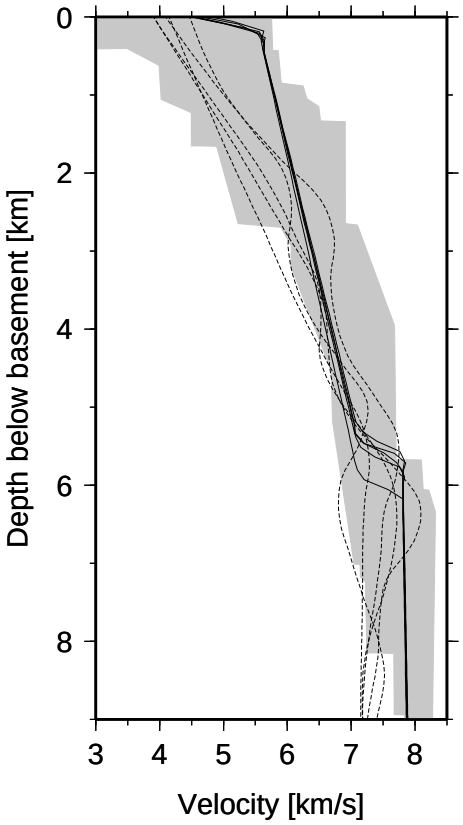

Figure 12.